# A software defined radio based method for accurate frequency estimation for space domain awareness in real-time.

**Edwin G. W. Peters**
*The University of New South Wales Canberra*
**Timothy Bateman**
*The University of New South Wales Canberra*

**Rabbia Saleem**
*The University of New South Wales Canberra*

**Melrose Brown**
*The University of New South Wales Canberra*

**Andrew Lambert**
*The University of New South Wales Canberra*

**August 2022**

**ABSTRACT**

We present our proposed software defined radio (SDR) algorithm that can estimate Doppler frequency measurements for space domain awareness purposes in real-time. We present the algorithm in detail and show estimation accuracy through simulation studies. Further, we show an example using captured radio frequency (RF) signals, where Doppler measurements obtained using our proposed SDR approach have been used for orbit determination of a satellite. The algorithm utilizes consumer grade graphics processing units (GPUs) to allow faster than real-time processing of captured RF signals.

## 1. INTRODUCTION

With the increased access to space and an increasing number of private launch and satellite providers, the space domain awareness (SDA) field has received increasing attention within the past decade [5, 14, 16]. The number of spacecraft is predicted to increase significantly over the next decade. Keeping pace with the rapidly growing population of active, maneuvering, civilian satellites, requires the development of new capabilities, including a civilian SDA sensor network, to support the next generation of space traffic management (STM) systems. One way to determine the orbit of satellites is using radio frequency (RF) measurements. Typically, ranging measurements are used by satellite operators, since these provide both frequency offset measurements due to the Doppler effect and round-trip time [7]. However, ranging measurements typically can only be used by the operator of the satellite. An alternative to ranging is mono- or bi- or multi-static radar. These however, require a high power transmitter to illuminate the targets and are costly to build. An alternative, more cost-effective, method is to utilize passive RF measurements, where ground-based receiver antennas capture spacecraft RF emissions, such as communications and beacons. In this work, we present a flexible software defined radio (SDR) based method that can perform high fidelity RF transmitter frequency offset measurements for those satellites that transmit as part of their normal operation.

Satellite ephemeris estimation from RF signals has been done using a variety of methods. These methods can mainly be separated into active methods, passive single station methods and passive multi-station methods. The active methods use a controlled illuminator, and consists typically of radar systems. The passive single station methods use merely a single station to receive the RF signals. When only a single aperture is used for receiving, the only direct information that can be extracted from the received RF signal is the frequency offset caused by the Doppler effect due to the relative velocity between the transmitter (satellite) and receiver (ground station) [2]. The Doppler frequency can be estimated

and can be used for orbit determination. Multiple co-located receivers at one receiver site can be used to determine the angle of arrival of an emitted signal. Passive multi-station methods utilize geographically dispersed receivers. With the appropriate synchronisation, the time and frequency of observations between stations will differ. The emitter's location can then be determined through the difference of the arrival frequencies and times as well as the geometry of the receivers. Typical methods within this category are time difference of arrival (TDoA) and frequency difference of arrival (FDoA) [4, 17]. The measurements obtained through the above methods can be used for orbit determination and refinement. This can be done through measurement models in orbit determination tools such as GMAT [10], Orekit [12] or STRF [3].

Spectral Doppler estimation techniques are frequently used. One spectral method is the coarse Doppler estimation through a grid search [22, 19]. While most of these coarse Doppler estimation methods estimate the Doppler frequency sufficiently for successful demodulation of the signals, the fit of spectral Doppler estimation methods is normally limited by the fast Fourier transform (FFT) bin resolution. However, interpolation techniques can be used for more accurate spectral estimations [1]. The Welch periodogram is fast to compute and, provided the signal to noise ratio (SNR) is sufficient, easy to analyze [9]. Tracking loops, such as a Costa's loop produce more accurate Doppler estimations [6, 11].

In this work, we propose to utilize matched filters to estimate the Doppler frequency of satellites. This method relies on a-priori information in the form of knowledge of the modulation scheme and symbol rate. One advantage of utilizing matched filters over tracking loops is that longer matched filters tend to be more accurate in low SNR situations. Further, the proposed method provides frequency estimates and quality of measurement through covariance measurements. The proposed method is inspired by our previous work [19], and spread spectrum based Doppler acquisition methods, such as [15, 20, 21].

This paper is organised as follows: In Section 2 we present background on the Doppler effect. This is followed by the presentation of our proposed two-stage Doppler estimation algorithm that performs a coarse estimation followed by a fine estimation in Section 3.2.1. Section 3.2 presents simulation studies to illustrate the Doppler estimation accuracy of the proposed algorithm for different SNRs. Simulations are presented in Section 4. Finally, in Section 5, we show a demonstration on a captured satellite signal and a orbit determination performed on the estimated frequency from captured satellite signals.

*Notation:* Let $\triangleq$ denote a definition or assignment. For simpler notation, we define multiplications of two length $n$ sequences as element wise. For example, let $a = [a_0, a_1, a_2] \in \mathbb{C}^3$ and $b = [b_0, b_1, b_2] \in \mathbb{C}^3$, then $ab = [a_0b_0, a_1b_1, a_2b_2] \in \mathbb{C}^3$.

## 2. BACKGROUND

Orbiting spacecraft exhibit an observed relative velocity from ground stations. This velocity is called the *range rate* and indicates the rate at which the spacecraft is approaching the ground station (negative) or departing the ground station (positive). The range rate is zero when the spacecraft is at its closest approach to the ground station. That is, the orbital velocity of the spacecraft and Earth's procession is orthogonal to the ground station range vector. Radio waves, like any other form of acoustic or electromagnetic (EM) wave exhibit Doppler effects when two objects are moving relative to each other. The Doppler frequency is given by

$$f_d = \frac{v_r}{\lambda} \tag{1}$$

and depends on the range rate $v_r$, measured in m/s, and the wavelength, which is given by

$$\lambda = \frac{c}{f_c}, \tag{2}$$

where $f_c$, measured in Hz, is the carrier frequency and $c = 299\,792\,458\,\mathrm{m/s}$ is the speed of light.

By measuring the Doppler frequency with respect to the carrier frequency $f_c$, the range rate can be estimated. The range rate is a many-to-one map, mapping the spacecraft's orbital motion into a single parameter. Thus, no unique spacecraft state exists for a single Doppler measurement. However, by observing the Doppler frequency over time, such as an entire pass or multiple passes, a spacecraft's orbit can be determined using batched least squares methods or Kalman filter [11] methods through OREKIT [13], GMAT [10], STRF [3] or other orbit determination tools. Fig. 1 shows an example of the orbit determination flow using a batched least squares method.

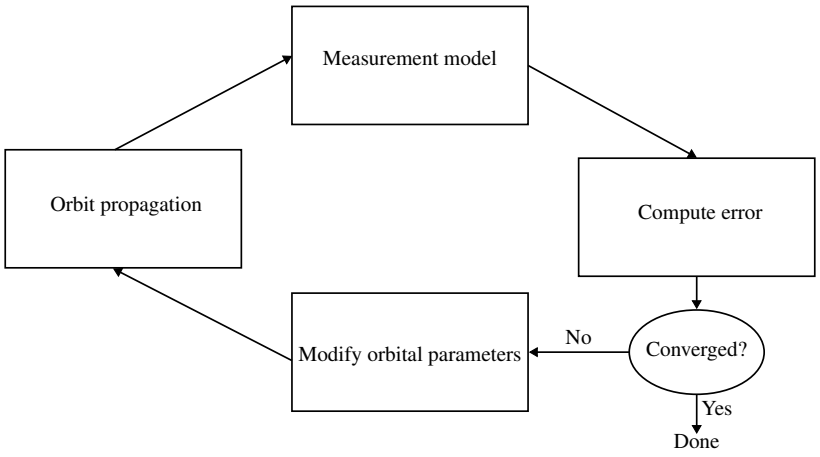


Fig. 1: Process flow for batched least squares orbit determination based on Doppler

## 3. MATCHED FILTER DOPPLER ESTIMATION

The proposed matched filter Doppler detection SDR method consists of a digitization followed by a two step Doppler detection and correction process, depicted in Fig. 2. The first step of the SDR is performed in the digitizer, which applies a RF level band pass filter, down conversion to intermediate frequency (IF) and digitization. Next, a coarse Doppler search is performed using a graphics processing unit (GPU)-based grid search, presented in our previous work [19], of which the source code is available on [18]. After the coarse Doppler estimation, a fine Doppler estimation is performed, which is heavily inspired by the principles of the correlation demodulator. This process yields a Doppler estimate for each symbol throughout a received modulated signal. This section will explain the different steps of the Doppler estimation in detail.

### 3.1 Digitization

The digitization is done using commercial of the shelf RF digitizers. We use the Ettus universal software radio peripheral (USRP) B210 and X310 series, as well as the BladeRF 2.0. The digitizer hardware is typically interfaced through GNU radio [8] which stores the recorded in phase and quadrature phase (IQ) data to a file or streams it to the Doppler frequency estimator through a socket. The digitizers are supplied with global navigation satellite system (GNSS) disciplined clocks and time sources for increased timing accuracy. Timing information is processed alongside the digitized IQ data.

### 3.2 Coarse Doppler estimation

The aim with the coarse Doppler estimation is to get a sufficiently precise Doppler estimate to avoid ambiguities in the fine Doppler estimation. The coarse Doppler estimation is performed by cross-correlating the received signal with templates of the expected modulated carrier with different Doppler frequency offsets. The coarse Doppler shift can then be found by locating the Doppler shifts that maximize the magnitude of the cross-correlations. Fig. 3 provides an overview of the coarse Doppler search algorithm.

For a received signal segment $x = [x(0), \cdots, x(m-1)] \in \mathbb{C}^m$ and filter $h = [h(0), \cdots, h(n-1)] \in \mathbb{C}^n$, where $n << m$, the valid part of a cross-correlation of the sequences is given by

$$c(x,h) = \text{xcorr}(x,h) \qquad \in \mathbb{C}^{m-n+1}, \tag{3}$$

where[1]

$$\text{xcorr}(x,h)(k) \triangleq (x \star h)(k+n-1) \qquad k = [n-1, n, \cdots, m-1] \tag{4}$$

$$= \sum_{\tau=0}^{n-1} x(k+n-1-\tau)h(\tau) \qquad k = [n-1, n, \cdots, m-1]. \tag{5}$$

[1]The group delay of the filter has to be taken into account when time stamping the final measurements.

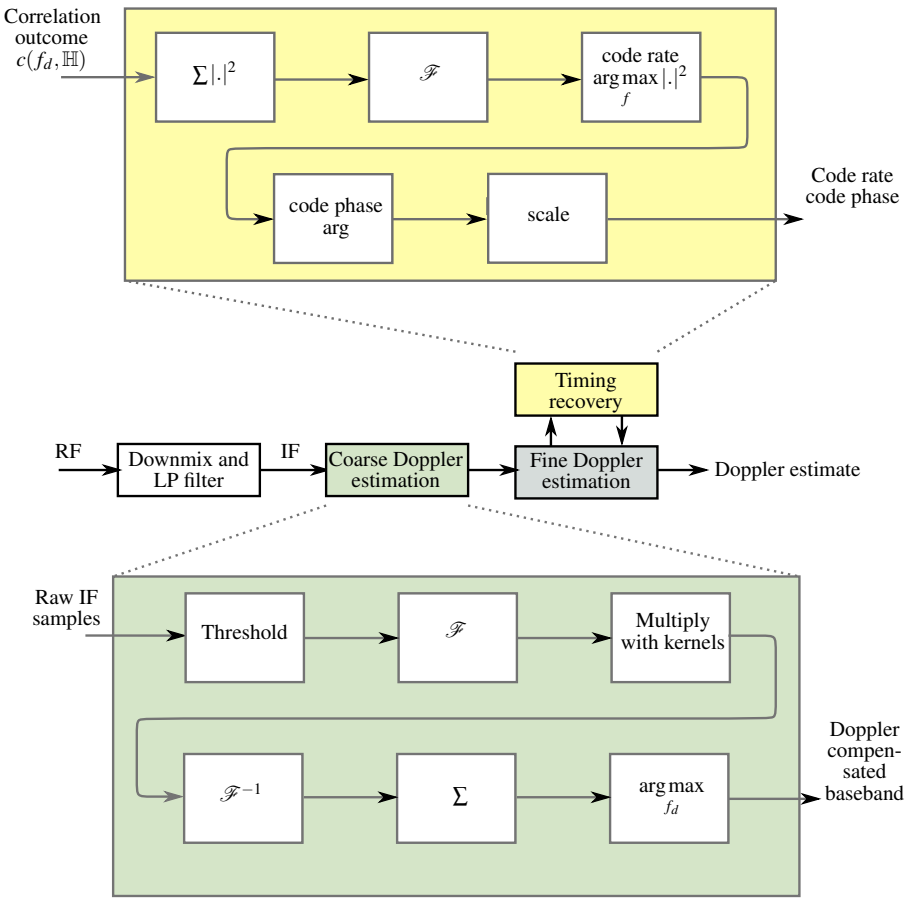


Fig. 2: Block diagram of the SDR used for the matched filter approach.

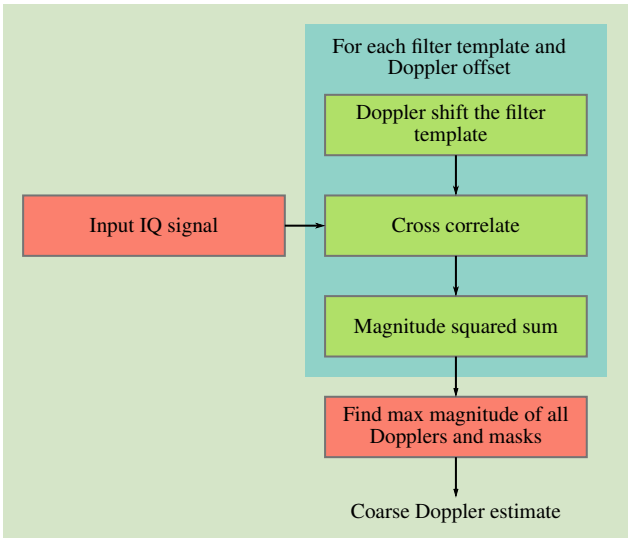


Fig. 3: Illustration of the computations in the coarse Doppler search. The blocks in the blue box are executed for each combination of Doppler offset and filter template. This can be done sequentially or in parallel.

This can be computed through fast convolution in the frequency domain as

$$c(x,h) = \mathscr{F}^{-1}\{X(f)H(f)\}, \tag{6}$$

where

$$X(f) \triangleq \mathscr{F}\{x\} = \sum_{k=-\infty}^{\infty} x(k)e^{-2\pi j\frac{k}{T}f} \tag{7}$$

$$H(f) \triangleq \mathscr{F}\{h\} \tag{8}$$

are the Fourier transforms of $x$ and $h$, respectively and $T$ is the sample interval. Note, the "valid" part of the cross-correlation in (3) are samples $[n-1,n,\cdots,m-1]$.

Let the signal $x(k)$ be given by

$$x(k) = r(k) + \omega(k), \tag{9}$$

where $r(k)$ is a base band (BB) signal $s(k)$ with unknown time-varying carrier remnants due to the Doppler shift

$$r(k) = s(k)e^{j2\pi f_d(k)\frac{k}{T}} \tag{10}$$

where $f_d(k)$ is the time-varying Doppler shift and $\omega(k)$ represents other disturbances, such as zero-mean white Gaussian noise and sporadic bursts. We let $h = [h(0),\cdots,h(n-1)] \in \mathbb{C}^n$ be a filter resembling a short segment of the emitted signal $s = [s(0),\cdots,s(n-1)] \in \mathbb{C}^n$. Then, the magnitude squared of the cross-correlation at sample 0

$$|c(x,h)(0)|^2 \tag{11}$$

will be maximized if

$$h = r = se^{j2\pi f_d\frac{1}{T}[0,1,\cdots,n-1]}, \tag{12}$$

where, for simplicity, the Doppler frequency $f_d$ is assumed to be constant within the correlation window. To find the Doppler frequency of the signal, we find the frequency offset $f_d$ for the filter $h$ that maximizes the sum of (3) as

$$f_d^\star = \arg\max_{f_d} \sum_{0}^{m-n} |c(x,h\cdot g(f_d))|^2, \tag{13}$$

where

$$g(f)(k) \triangleq e^{j2\pi f\frac{1}{T}[k,k+1,\cdots,k+n-1]} \tag{14}$$

and $g(f) \triangleq g(f)(0)$, with $n$ being the length of the filter $h$.

It is worth noting, that in (13), we assume the Doppler frequency $f_d$ to be constant. Both orbit simulations and practical results show, that the Doppler changes are sufficiently small within short time frames[2], which provides good cross-correlation results when performing the coarse Doppler search over shorter sequences of signal.

### 3.2.1 Coarse Doppler acquisition implementation

For the coarse Doppler acquisition, it is often desirable to use multiple filters. When nothing but the modulation scheme and bandwidth are known of the signal $r$, one would typically select a filter length in number of symbols, and generate a filter $h$ for each possible symbol sequence. This would result in

$$N_{\text{filters}} = N_{\text{symbols}}^{N_{\text{filter\_length\_symbols}}} \tag{15}$$

being needed, where $N_{\text{symbols}}$ is the number of symbols in the modulation constellation and $N_{\text{filter\_length\_symbols}}$ is the filter length in symbols.

[2]The length of the time frames are relative to the carrier frequency $f_c$. For higher carrier frequencies the Doppler increases. However, higher carrier frequencies tend to utilize significantly higher signal bandwidths and symbol rates. Due to this, the phase change within one matched filter correlation for a fixed number of symbols will be less as the symbol rate increased. This makes the coarse Doppler estimation less sensitive to larger frequency changes within a processing sequence.

**Remark 1.** *It is worth noting, that the Doppler search also can be performed successfully by only using a subset of the filters as it is not necessary to match all symbol patterns, and in modulation schemes such as phase shift keying (PSK) some filters are inverted versions of others. Alternatively, if for example a synchronization sequence or other repetitive part of a signal is known, it might suffice to only utilize that sequence for the coarse Doppler acquisition, reducing the computational requirements significantly.*

Define the set $\mathbb{H} \triangleq \left[h_0, h_1, h_{N_{\text{filters}}-1}\right]$ as the set of filters. We then compute the cross-correlation magnitude as

$$c_{\text{mag}}(f) = \sum_{h\in\mathbb{H}} \sum_{k=0}^{m-n} |c(x, h\cdot g(f))(k)|^2, \tag{16}$$

where $g$ is defined in (14). The graph in the coarse Doppler estimation block in Fig. 5 shows a graphical illustration of $c_{\text{mag}}(f)$. The coarse Doppler frequency is then found by

$$f_{d,\text{coarse}} = \arg\max_{f\in\mathbb{F}} c_{\text{mag}}(f) \tag{17}$$

$$= \arg\max_{f\in\mathbb{F}} \sum_{h\in\mathbb{H}} \sum_{k=0}^{m-n} |c(x, h\cdot g(f))(k)|^2, \tag{18}$$

where $\mathbb{F}$ is the set of Doppler frequencies to search over. It is worth noting that (18) is a combinatorial problem, since (16) has to be computed for every frequency $f \in \mathbb{F}$. For that reason, the set $\mathbb{F}$ is initialized as a bounded discrete set, with the highest and lowest frequencies being estimated from orbital parameters of the spacecraft or, if the orbit is unknown, bounded by the sample rate $f_s$ of the signal, and the step size being

$$f_{\text{step}} = \frac{1}{4} N_{\text{filter\_length\_symbols}} \frac{f_{\text{sym}}}{f_{\text{dmax}}}, \tag{19}$$

where $f_{\text{sym}}$ is the symbol rate of the signal and $f_{\text{dmax}}$ is the maximum expected Doppler frequency. This allows at most $\frac{\pi}{4}$ radians of phase wrap of error between two filters in $\mathbb{F}$, preserving 90 % of the correlation energy.

It is worth noting, that the higher the symbol rate of the signal is compared to the maximum expected Doppler frequency or sample rate, the smaller the set $\mathbb{F}$ needs to be. In fact, when the symbol rate of the signal significantly exceeds the maximum expected Doppler frequency, the coarse Doppler search can be omitted.

For the implementation of the coarse Doppler acquisition, the two frequencies that result in the highest and second highest value in (16) are found. A weighted average between these is then selected as the coarse Doppler estimate. The length of the signal blocks is selected such that the Doppler frequency change within a block is small, typically within a few Hertz per block at the time of closest approach (TCA) (where the Doppler is changing the fastest). The coarse Doppler estimates generated through this are sufficiently accurate to resolve any phase ambiguities in the fine Doppler estimation. Practically, a suitable block length is typically around 300 ms to 400 ms duration.

To accelerate the processing and take advantage of the fast convolution (3), which uses the FFT algorithm, the coarse Doppler estimation is performed block-wise over the signal. The algorithm is depicted in Fig. 3 and is implemented in CUDA to take advantage of GPU acceleration.

As is in the name, the coarse Doppler search is not intended to find the exact frequency offset. Instead, the frequency offset needs to be estimated sufficiently accurate, that a fine Doppler search can estimate and remove the remaining Doppler.

### 3.3 Finding packet boundaries

In (18), we found the frequency where the signal is present. Before performing the fine Doppler estimation, it is required to find potential packet boundaries. This is necessary, since the phase and sample locations are not necessarily coherent between packets, even when these are closely spaced. The fine frequency estimation can then be performed packet-wise.

The packets are found by determining where the signal magnitude exceeds a threshold. This threshold $q$ is typically chosen as a scalar multiple of the noise magnitude, typically measured out of band though the FFT or by correlating

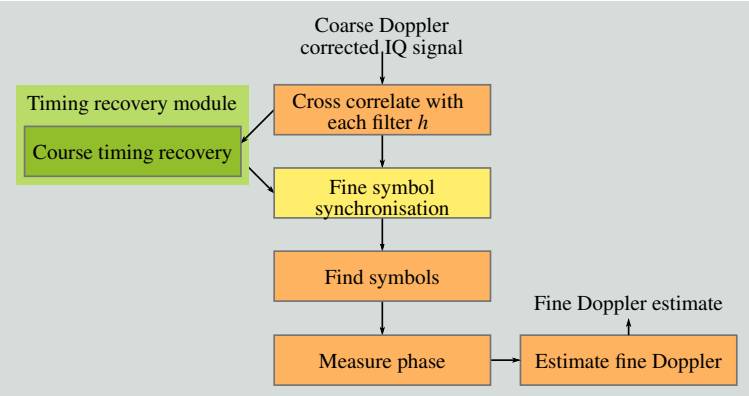


Fig. 4: Fine Doppler estimation flow graph

the same filters with frequency offsets that are known to be out of band. The packets location are then found by the samples that satisfy

$$L_{\text{burst}} = \left\{ k \colon \left[ \sum_{h \in \mathbb{H}} |c(x, h \cdot g(f_d))(k)| \right] > q \right\}, \tag{20}$$

where $f_d$ is the coarse Doppler frequency found using (18) Practically, there might be parts of the packet between two symbol sample locations where the magnitude of $c$ is lower than the threshold $v$. Here one can either parse the set $L_{\text{burst}}$ and consider gaps between samples below a certain threshold as belonging to a single burst, or one could low-pass filter $\sum_{h \in \mathbb{H}} c(x,h)$ prior to the thresholding.

An example of the magnitude output of the Doppler search is shown on the left in Fig. 5, where a modulated signal is found with a Doppler offset of around 22 kHz. The transmission starts at around sample 20 000. The coarse Doppler estimation is fully implemented in CUDA and executes in real-time on consumer grade GPUs.

### 3.4 Fine Doppler estimation

The fine Doppler estimation is performed on each burst that is found in the coarse Doppler estimation. If no bursts are found, the fine Doppler estimation is skipped for that block. The fine Doppler estimation consists of multiple steps as depicted in Fig. 4. First, the symbol correlation is performed. This is followed by a timing acquisition to find the symbol locations, explained in Section 3.5. Next, the phase of the symbols that maximize the correlation magnitude is found. The final step consists of the estimation of the phase rate (frequency) based on the symbol phase measurements.

After the coarse Doppler estimation is performed on a signal sequence, the coarse Doppler is removed from the signal

$$x_d(k) = x(k) e^{-j2\pi f_{d,\text{coarse}} \frac{k}{T}}, \tag{21}$$

and the fine Doppler estimation commences. For the fine Doppler estimation, a "soft correlator demodulation" is performed, where a set of filters $\mathbb{H}$ are correlated onto the signal. Each filter in $\mathbb{H}$ covers a unique combination of symbols, and the cardinality of $\mathbb{H}$ is $N_{\text{filters}}$, as computed in (15).

Each of the filters $h \in \mathbb{H}$ are correlated with $x_d$. For each filter, the cross-correlation (3) is computed. At each sample, the filter with the maximum magnitude indicates the symbol number

$$s(k) = \arg\max_{h \in \mathbb{H}} |c(x_d, h)(k)|. \tag{22}$$

When the locations of the symbols are known, (22) only has to be computed for the symbol locations $k_n$. An example of the magnitude of the correlations of the individual filters of a set with $N_{\text{filters}} = 4$ (binary PSK (BPSK)) is depicted in the fine Doppler estimation block in Fig. 5.

Next, the phase $\phi$ is computed for each of the known symbol locations

$$\phi(k_n) = \angle c(x, h_{s(k_n)})(k_n), \tag{23}$$

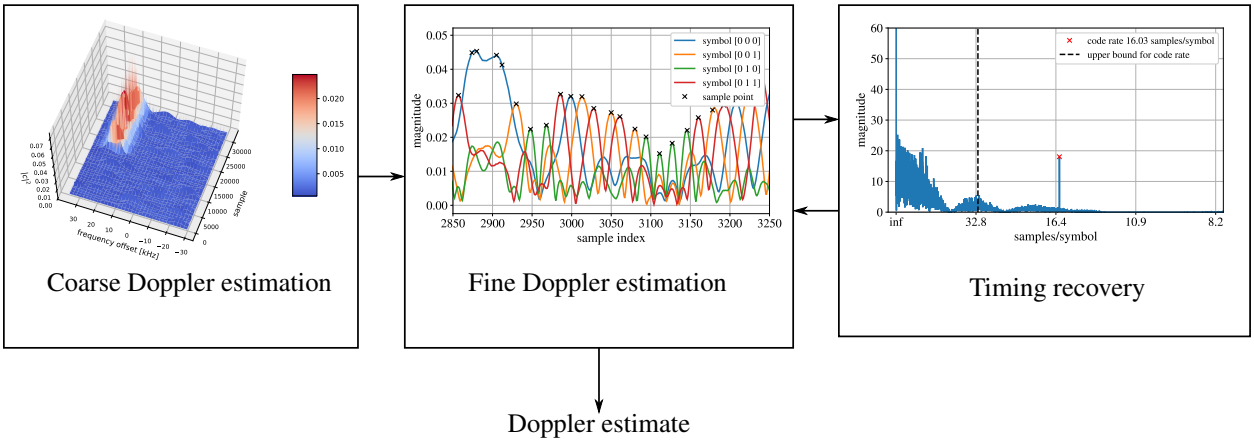


Fig. 5: Flow of the coarse and fine Doppler estimation and the timing recovery modules with graphical visualizations.

where $\angle x$ is the complex argument of $x \in \mathbb{C}$. The difference in phase between two consecutive symbols yields the remaining Doppler frequency

$$f_d(k_n) = \frac{\phi(k_n) - \phi(k_{n-1})}{k_n - k_{n-1}} \frac{1}{f_s} + f_{d,\text{coarse}}, \tag{24}$$

where $k_{n-1}$ indicates the sample of the previous symbol. Care has to be taken when computing (24) if symbol wrap occurred. Resolving the coarse Doppler search with a frequency spacing as set by (19) avoids ambiguities.

For digitized RF signals, which typically are affected by oscillator drift and uncertainties between receivers and transmitters among other effects such as noise and interference, the symbol-wise frequency estimation is too sensitive for accurate estimations. Instead a "de-noised estimate" of the Doppler frequency is obtained over a group of symbols, typically a single burst or a cut of a long burst ranging from 500 to 5000 symbols. This is done by measuring the phase for each symbol using (23), unwrapping the phase and performing a least squares curve fit of a quadratic function to the measured phase.

**Remark 2.** *It is worth noting that a quadratic function is not an optimal fit for a Doppler curve that represents a sigmoid function. However, for short sequences of the signal, a quadratic function provides a good fit without overfitting to the noise and disturbances. Future work will investigate different de-noising methods for the fine Doppler estimation.*

The phase can have ambiguities when some of the filters merely are a sign reversal or a conjugate of each other. This can result in $\pi$ or $\pm\frac{\pi}{2}$ rad of phase jumps. These have to be removed prior to the denoising. For frequency shift keying (FSK) with a carrier spacing of half the symbol rate and BPSK, the ambiguity removal function is given by

$$\phi_u(k_n) = ((\phi_{k_n} + \pi)\,\%\pi) - \frac{\pi}{2}, \tag{25}$$

where % is the remainder after division operator. Empirical results show that a second order polynomial produces accurate results. The fitted polynomial can then be used to produce accurate Doppler frequency estimations within the time of the group of symbols.

A graphical visualisation of the fine frequency estimation is illustrated in Fig. 6. The first block selects the symbols using (22). While the symbol value $s$ is discarded, the phase of the correlation at $s(k)$ is computed using (23). The phase is illustrated in the second block in Fig. 6 with the green squares. Due to the modulation scheme, which for this example is FSK, the phase jumps with $\pi$. This is compensated using (25), resulting in the blue dots. The phase is unwrapped and the rate of change is estimated. The unwrapped phase and a second order curve fit are shown in the third block in Fig. 6. The last block in Fig. 6 shows the symbol phase (zoomed out version of the blue dots in the second block) after the coarse correction (blue) and coarse plus fine correction in red. A horizontal line after the coarse and fine Doppler correction indicates that the frequency offset has been successfully removed.

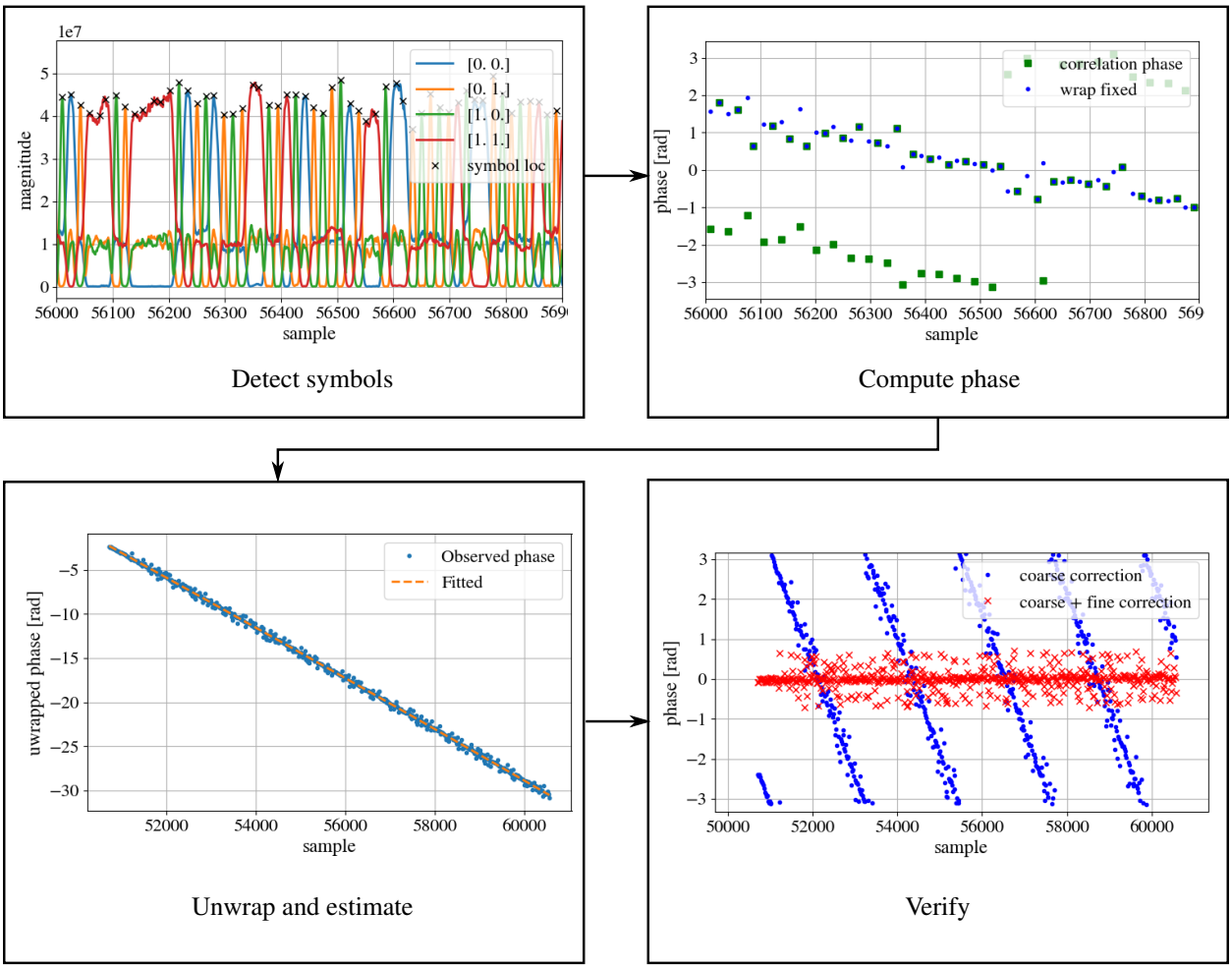


Fig. 6: Visual flow with figures of the fine frequency estimation.

**Remark 3.** *Care has to be taken when performing the unwrap operation on the symbols. Especially low SNR scenarios or large amounts of interference in the signal can result in invalid unwraps occurring. Many of the invalid unwraps can be detected and removed using robust phase unwrapping algorithms. These are however out of the scope of this work.*

### 3.5 Timing recovery

Part of the fine Doppler estimation is the timing recovery. The timing recovery finds the locations $k_n$ of the symbols within a sequence of signal. The magnitude of the individual filter correlations in the fine Doppler estimation block in Fig. 5 illustrate a regular pattern of peaks. It is also worth noting, that while one of the peaks has the highest magnitude (the peak where the filter matches the signal), the magnitude of the cross-correlations of the signal with other filters still exhibit a similar frequency in their oscillations. For the timing recovery, we estimate the frequency and the phase of these oscillations. This is done using a Fourier method. The steps involved in the timing recovery algorithm are depicted in the flowchart in Fig. 7.

First, the cross-correlation of all the symbols after the coarse Doppler frequency offset correction is performed are summed together to maximize the energy in the peaks at each sample

$$v(k) = \sum_{h \in \mathbb{H}} |c(x_d, h)(k)|^2. \tag{26}$$

Next, the Fourier transform $V = \mathscr{F}(v)$ is computed. The one-sided magnitude of $V$ is depicted in the timing recovery

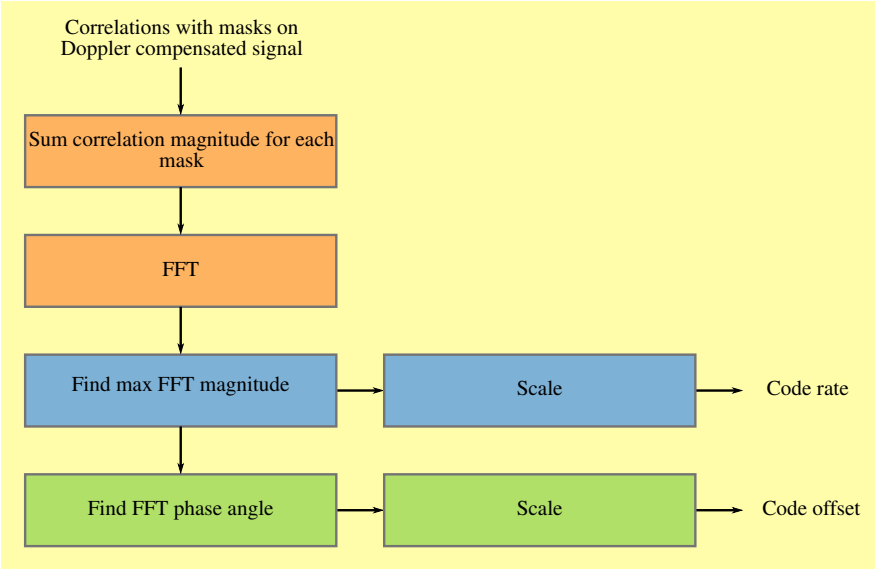


Fig. 7: Illustration of the timing recovery process, which is done using a code rate and phase search in the frequency domain.

block in Fig. 5. Here a clear peak appears that indicates the symbol spacing in samples. It is worth noting, that there is a large number of low frequency and DC content present in $V$, so a lower bound for the symbol rate has to be specified.

Let $i^\star$ be the index in the one-sided $N$-point FFT that satisfies

$$i^\star = \arg\max_{i \in \mathbb{S}} |V(i)|^2, \tag{27}$$

where the interval $\mathbb{S} = ]p, \frac{N}{2} - 1]$ represents the sequence of scaled code rates. The upper expected oversampling rate $p$ limits the code rate estimation range and is configured such that DC and low frequency content is excluded in (27).

Next, the actual code rate and code offset in samples can be found through scaling. The code rate $r$ is given by

$$r = \frac{N}{i^\star}, \tag{28}$$

while the code delay is found by

$$\phi = \frac{r \angle V(i^\star)}{2\pi}. \tag{29}$$

## 4. SIMULATION RESULTS

Simulation studies are used to verify the accuracy of the proposed algorithm. The range rate is determined for a low Earth orbit (LEO) satellite pass, for which a Doppler curve is computed using interpolation. Random data in packets sized between 500 to 8000 symbols with random spacing is modulated in FSK and BPSK. These are Doppler shifted to represent a satellite pass and different levels of noise has been added to achieve SNRs in the range of 0 dB to 14 dB. The proposed algorithm is then used to process the generated data and the estimated range rates are compared to the generated values. The pass length is 12 minutes. The centre frequency $f_c = 450$ MHz and the symbol rate is 7500 Hz using FSK and BPSK modulation schemes. An oversampling rate of 16 has been used. The mean absolute error (MAE) is used to measure the error and is given by

$$\mathrm{MAE}(x,y) \triangleq \frac{1}{N} \sum_{k=0}^{N-1} |x(k) - y(k)|, \tag{30}$$

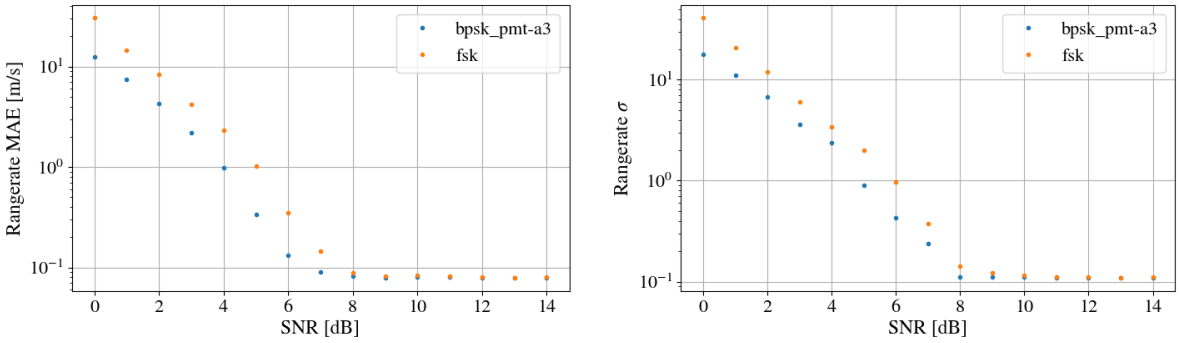


Fig. 8: The MAE and standard deviation of the Doppler estimation SDR algorithm for FSK and BPSK modulation schemes.

where $x, y \in \mathbb{C}^N$.

Fig. 8 shows the MAE of the estimated rangerate compared to the rangerate used to generate the test signal. The MAE and standard deviation decrease with increasing SNR and asymptotically approach 0.07 m/s MAE and 0.1 m/s standard deviation at SNR levels of 8 dB and above. The reason that the accuracy is not increasing past 8 dB SNR is due to the curve fitting method to estimate the fine frequency offset. Future research will investigate higher accuracy methods. The sensitivity and accuracy of the smoothing method is a tradeoff between acceptable performance in low SNR settings and high accuracy at high SNR settings. Since low gain omni-directional antennas are used for current data collection campaigns, the sensitivity is tuned towards low SNR settings.

It is further worth noting, that a consumer-grade computer using a Nvidia GTX 1060 GPU performed the coarse and fine Doppler estimation for the entire 12 minute pass in less than 3 minutes using less than 50 % of the GPU resources.

The block size was set to 65 536 samples (553 ms), the search grid was ranging from −11 250 Hz to 11 250 Hz with a spacing of 225 Hz, corresponding to 0.06 Hz per filter fir FSK and 0.09 Hz per filter for BPSK. This resulted in the cardinality of $\mathbb{F}$ being 100. The cardinality of the filter set $\mathbb{H}$ was 4 for FSK with each filter being two symbols long. For BPSK, the cardinality of $\mathbb{H}$ was 4 with each filter being three symbols long, but not containing sign-reversed templates of the symbol sequence. For example the sequence $[1,1,0]$ is the a $\pi$ rad rotated version of $[0,0,1]$ and can be omitted for BPSK.

## 5. EXAMPLES

The proposed SDR algorithm is actively used for frequency estimation of satellites. Figs. 9 to 11 show a spectrogram with estimated frequency overlay, estimated SNR and the covariance parameters of the Doppler estimation for a single pass of the LEO satellite Saral. In Fig. 9, the colour intensity indicates the standard deviation for the fine Doppler estimation of each burst or cut sequence of the received signal. The standard deviation is computed based on the residual of the de-noised curve fit to the data points. It is worth noting the correlation between a higher standard deviation in Fig. 9 to a lower SNR in Fig. 10 and higher covariance parameters in Fig. 11. The covariance parameters in Fig. 11 are from the curve fit of the quadratic function $ax^2 + bx + c$.

Figure 12 shows the range rate residual of two consecutive passes after performing an orbit determination using range rate measurements obtained using the proposed SDR algorithm. The orbit determination is performed using GMAT. Table 1 shows the average residual and standard deviation across all data points for each iteration. The orbit determination residuals after the fourth iteration are an order of magnitude larger than the MAE of the SDR algorithm shown in Fig. 8.

## 6. CONCLUSION

We presented an SDR-based frequency estimation algorithm that utilizes a bank of matched filters. The frequency estimation is performed in two stages. The coarse Doppler grid search is implemented on a GPU, allowing faster

| Iteration | MAE [m/s] | $\sigma$ [m/s] |
|---|---|---|
| 0 | 82.443 | 63.02 |
| 1 | 5.703 | 4.376 |
| 2 | 0.618 | 0.79 |
| 3 | 0.502 | 0.795 |

Table 1: MAE and standard deviation of the orbit determination.

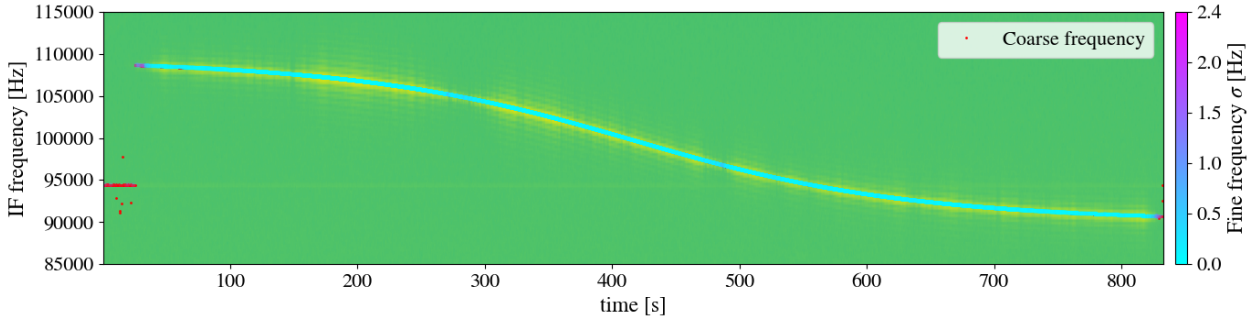


Fig. 9: Spectrogram of Saral (NID 39086) with coarse and fine frequency estimation overlayed. The colour intensity of the fine estimate indicates the standard deviation.

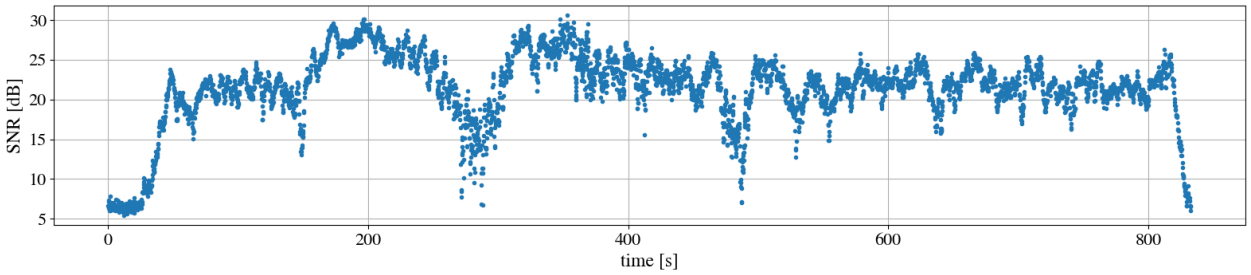


Fig. 10: Estimated SNR for Saral (NID 39086).

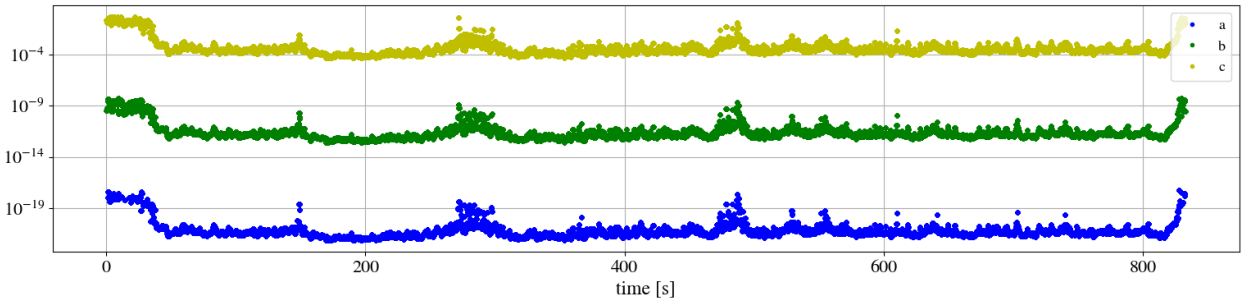


Fig. 11: The covariance parameters for the second order piece-wise fine frequency estimation for Saral (NID 39086).

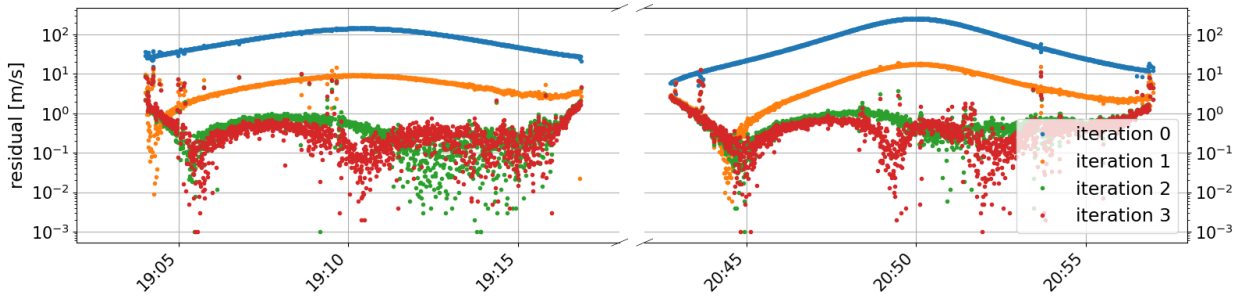


Fig. 12: Residual after four iterations of an orbit determination for Saral (NID 39086).

than real-time processing on consumer grade GPUs. Simulation results show, that using second order curve fits as the smoothing method for the fine frequency estimation, the range rate (based on Doppler) can be successfully estimated with an MAE down to 0.07 m/s at SNRs above 8 dB. The algorithm has been applied to satellite data recorded using SDR hardware, and initial studies of orbit determinations have been performed successfully, with the range rate MAE close to 0.5 m/s.

Future work will investigate more advanced signal smoothing and estimation methods, as well as the application of robust phase unwrapping methods, which allows more accurate Doppler estimation in low SNR settings.


[1] Elias Aboutanios. *Frequency Estimation for Low Earth Orbit Satellites*. PhD thesis, University of Technology, Sydney Faculty of Engineering (Telecommunications Group), 2002.

[2] I. Ali, N. Al-Dhahir, and J. E. Hershey. Doppler characterization for LEO satellites. *IEEE Transactions on Communications*, 46(3):309–313, Mar 1998.

[3] Cees Bassa. STRF: satellite tracking toolkit for radio observations (RF) toolbox, 2020. `https://github.com/cbassa/strf`.

[4] Liu Congfeng and Yun Jinwei. A joint TDOA/FDOA localization algorithm using bi-iterative method with optimal step length. *Chinese Journal of Electronics*, 30(1):119–126, 2021.

[5] Giacomo Curzi, Dario Modenini, and Paolo Tortora. Large constellations of small satellites: A survey of near future challenges and missions. *Aerospace*, 7(133), 2020.

[6] Farzan Farhangian and RenÃ© Landry. Multi-constellation software-defined receiver for doppler positioning with LEO satellites. *Sensors*, 20(5866), 2020.

[7] Cyrus Foster, Henry Hallam, and James Mason. Orbit determination and differential-drag control of planet labs cubesat constellations. *ArXiv*, 2015.

[8] GNU Radio Website, accessed August 2022. `http://www.gnuradio.org`.

[9] Mohd Noor Islam, Thomas Q. Wang, Samuel Wade, Travis Bessell, Tim Spitzer, and Jeremy Hallett. Doppler and angle of arrival estimation from digitally modulated satellite signals in passive RF space domain awareness. In *Advanced Maui Optical and Space Surveillance Technologies Conference*, 2021.

[10] Moriba Jah, Steven Hughes, Matthew Wilkins, and Tom Kelecy. The general mission analysis tool (GMAT): A new resource for supporting debris orbit determination, tracking and analysis. In *Proceedings of the Fifth European Conference on Space Debris*, 2009.

[11] Joe J. Khalife and Zaher M. Kassas. Receiver design for doppler positioning with leo satellites. In *ICASSP 2019 - 2019 IEEE International Conference on Acoustics, Speech and Signal Processing (ICASSP)*, pages 5506–5510, May 2019.

[12] Luc Maisonobe, Pascal Parraud, Maxime Journot, and Albert Alcarraz-Garcia. Multi-satellites precise orbit determination, an adaptable open-source implementation. In *2018 SpaceOps Conference*, 2018.

[13] Luc Maisonobe, Véronique Pommier, and Pascal Parraud. Orekit: An open source library for operational flight dynamics applications. In *4th International Conference on Astrodynamics Tools and Techniques*, pages 3–6, 2010.

[14] NASA. Orbital debris, May 2021. `nasa.gov/mission_pages/station/news/orbital_debris.html`.

[15] Mohammad Neinavaie, Joe Khalife, and Zaher M. Kassas. Blind doppler tracking and beacon detection for opportunistic navigation with LEO satellite signals. In *2021 IEEE Aerospace Conference (50100)*, pages 1–8,

Mar 2021.
[16] Union of Concerned Scientists. Satellite database, May 2022. https://www.ucsusa.org/resources/satellite-database.
[17] Brian O'Keefe. Finding location with time of arrival and time difference of arrival techniques. *ECE Senior Capstone Project*, 2017.
[18] Edwin G. W. Peters. pyCuSDR: a GPU accelerated software defined radio with real time Doppler correction, July 2021. https://github.com/epeters13/pyCuSDR.
[19] Edwin G. W. Peters and Craig R. Benson. A Doppler correcting software defined radio receiver design for satellite communications. *IEEE Aerospace and Electronic Systems Magazine*, 35(2):38–48, Feb 2020.
[20] G. J. R. Povey and J. Talvitie. Doppler compensation and code acquisition techniques for LEO satellite mobile radio communications. In *Fifth International Conference on Satellite Systems for Mobile Communications and Navigation, 1996.*, pages 16–19, May 1996.
[21] S. U. Qaisar and C. R. Benson. Processing cost of doppler search in GNSS signal acquisition: Measuring doppler shift in navigation satellite signals. *IEEE Signal Processing Magazine*, 34(5):53–58, Sep 2017.
[22] Zhaowei Zhang, Hui Liu, Jun Yin, and Xiaoye Shi. Clustering-FFT based doppler-shift acquisition for space communications. *IEEE Transactions on Communications*, 70(2):1168–1182, Feb 2022.